ACS APPLIED MATERIALS & INTERFACES

Research Article

www.acsami.org

Effect of Covalent Modification of Graphene Nanosheets on the Electrical Property and Electromagnetic Interference Shielding Performance of a Water-Borne Polyurethane Composite

Sheng-Tsung Hsiao,[†] Chen-Chi M. Ma,*[,†] Hsi-Wen Tien,[†] Wei-Hao Liao,[†] Yu-Sheng Wang,[†] Shin-Ming Li,[†] Chih-Yu Yang,[†] Sheng-Chi Lin,[†] and Ruey-Bin Yang[‡]

[†]Department of Chemical Engineering, National Tsing-Hua University, Hsin-Chu 30013, Taiwan, ROC

[‡]Department of Aerospace and Systems Engineering, Feng Chia University, Taichung, Taiwan, ROC

Supporting Information

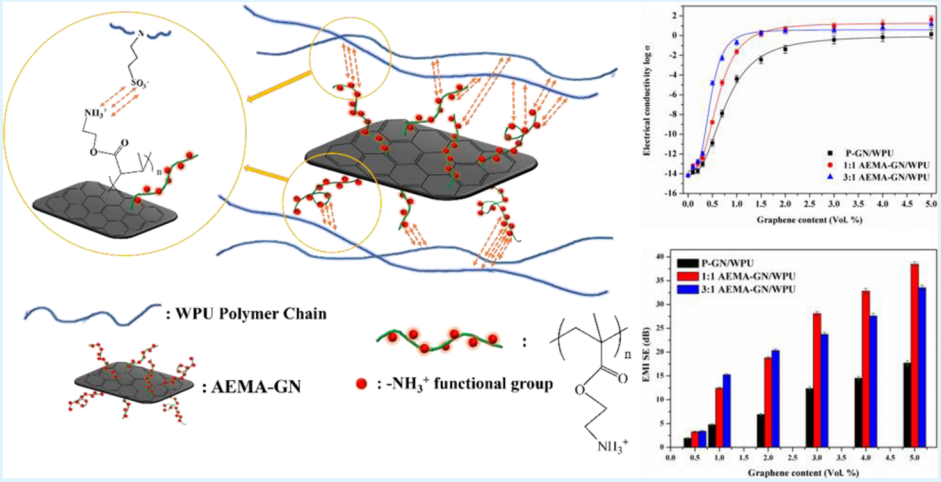

ABSTRACT: Flexible and lightweight graphene nanosheet (GN)/waterborne polyurethane (WPU) composites which exhibit high electrical conductivity and electromagnetic shielding performance were prepared. Covalently modifying GNs with aminoethyl methacrylate (AEMA; AEMA-GNs) through free radical polymerization effectively inhibited the restacking and aggregation of the GNs because of the $-NH_3^+$ functional groups grafted on the AEMA-GNs. Moreover, the AEMA-GNs exhibited high compatibility with a WPU matrix with grafted sulfonated functional groups because of the electrostatic attraction, which caused the AEMA-GNs to homogeneously disperse in the WPU matrix. This homogeneous distribution enabled the GNs to form electrically conductive networks. Furthermore, AEMA-GNs with different amounts of AEMA segments were introduced into the WPU matrix, and the effects of the surface chemistry of the GNs on the electrical conductivity and EMI shielding performance of composites were investigated. AEMA-GN/WPU composites with a GN loading of 5 vol % exhibited remarkable electrical conductivity (approximately 43.64 S/m) and EMI shielding effectiveness (38 dB) over the frequency of 8.2 to 12.4 GHz.

KEYWORDS: *graphene nanosheet, water-borne polyurethane, polymer composite, electromagnetic interference shielding, electrical conductivity, covalent modification*

1. INTRODUCTION

Electromagnetic interference (EMI) has become a considerable problem in the development of optoelectronic devices, sensitive electronic devices, densely packed systems, aircraft, spacecraft, and automobiles because of the increasing use of high operating frequencies and bandwidths,[1−3] especially the X-band (8.2−12.4 GHz) in electronic systems. Thus, considerable attention has been focused on the development of EMI shielding materials. The materials used in EMI shielding applications must be lightweight, inexpensive, flexible, and easy to process. A previous study[4] indicated that metals and metallic composites are the most commonly used materials for EMI shielding because of their excellent electrical conductivities. However, metallic materials are bulky and difficult to process. Although metallic materials can be coated on the surfaces of lightweight materials by using electroplating, electroless plating, or vacuum deposition approaches for EMI shielding applications,[5] these materials exhibit problems associated with chemical resistance,

Received: November 18, 2014
Accepted: January 8, 2015
Published: January 8, 2015

DOI: 10.1021/am508069v
ACS Appl. Mater. Interfaces 2015, 7, 2817−2826

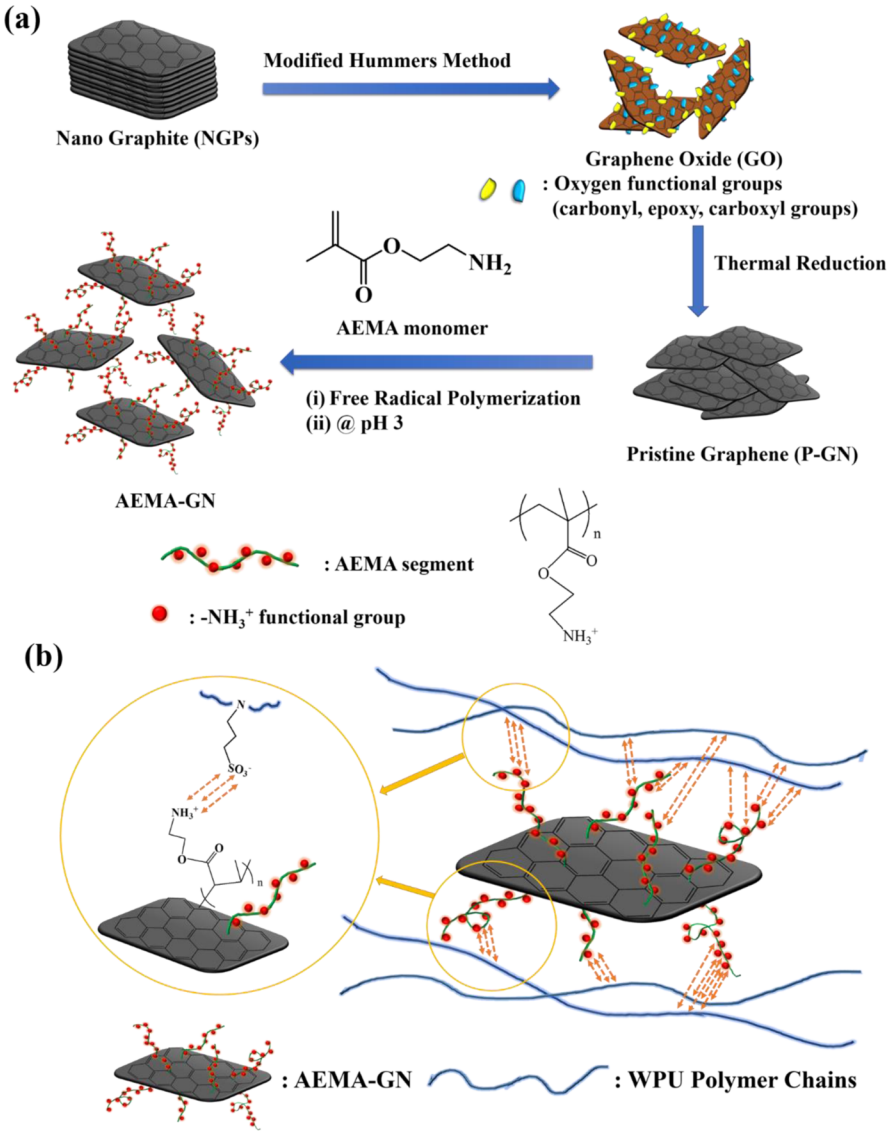

Figure 1. (a) Scheme of the procedure for preparing P-GN and AEMA-GN. (b) The AEMA-GN attached to the sulfonated functional groups of WPU through electrostatic attraction for better compatibility.

oxidation, corrosion, high density, and difficulty in processing. Conductive polymer composites are potential substitutes for metal-based materials.[6] Compared to metal-based EMI shielding materials, electrically conductive polymer composites are lightweight, resistant to corrosion, flexible, and easy to process, and they are suitable and effective for EMI shielding applications for aircraft, automobiles, and flexible electronic devices.[5,7]

The EMI shielding efficiency (EMI SE) of a polymer composite primarily depends on the intrinsic electrical conductivity, aspect ratio, and content of the fillers.[5,8−12] Graphene nanosheets (GNs), which are composed of 2D honeycomb lattices of carbon atoms, are extremely thin nanomaterials, and they have attracted a considerable amount of attention from researchers because of their ultrahigh mechanical properties and excellent electrical and thermal conductivities.[13,14] Therefore, the use of GN/polymer composites has been proposed for achieving high EMI shielding properties.[6,10,15,16] The addition of GNs, which form electrically conductive networks, enables the insulating polymer matrix to become electrically conductive and exhibit EMI SE. However, GNs usually exhibit poor compatibility with the polymer matrix, leading to severe restacking and aggregation of GNs in the polymer matrix. It is difficult to achieve the maximum enhancement in physical properties, especially electrical conductivity, through GNs without a homogeneous dispersion of GNs and strong interfacial interactions between the GNs and polymer matrix.[17,18] To date, few studies have investigated the effect of the dispersion state of GNs on EMI shielding performance. To improve the compatibility between GNs and polymer matrices and to obtain a stable dispersion of GNs in polymer matrices, modification of the GN surface is a useful method, including covalent bonding and noncovalent interactions. Covalent modification achieved by grafting organic functional groups onto the GN surface facilitates strong interactions between GNs and the polymer matrix.[19,20] However, the organic segments grafted on the GN surface typically destroy the structure of GNs and limit reinforcements of the electrical conductivity of the GN composite.[21,22] In contrast, noncovalent modification of GNs involves $\pi-\pi$ interaction or van der Waals force.[23,24] On the basis of our previous work,[25] the use of a noncovalent modification to

DOI: 10.1021/am508069v
ACS Appl. Mater. Interfaces 2015, 7, 2817−2826

modify GN through the adsorption of a cationic surfactant can effectively improve the compatibility with the polymer matrix without destroying the graphitic structure of GN. However, the interaction between the surfactant and GNs is weak, which causes the GN dispersion to be unstable during the preparation of polymer composites.[19] This study proposes a covalent modification of GNs that facilitates strong interactions with the polymer matrix. Additionally, to prevent the aforementioned problem of covalent modification from occurring, the degree of modification and the integrity of GNs are important issues for discussion.

The development of environmentally friendly polymeric materials that exhibit desirable properties is a global research focus. Waterborne polyurethane (WPU) is particularly noteworthy[26−28] because of its environmentally friendly preparation process, excellent mechanical performance, and ease of film formability. The grafted hydrophilic groups, such as sulfonic functional groups[28,29] or carboxyl functional groups,[30,31] make WPU negatively charged and homogeneously dispersed in aqueous solution. In addition, the chemical structures of the soft and hard segments of WPU can be easily controlled to obtain favorable properties and to satisfy application requirements.

In this study, GNs were fabricated using thermal reduction, and an effective chemical modification was achieved through free radical polymerization to prepare aminoethyl-methacrylate-grafted GNs (AEMA-GNs). Figure 1a shows the reaction procedure. In acidic solution, the amine functional groups ($-NH_2$) of the AEMA segments on the AEMA-GNs became positively charged ($-NH_3^+$), facilitating the homogeneous dispersion of the GNs in aqueous solution and preventing the GNs from aggregating through electrostatic repulsive interactions. When AEMA-GNs were introduced into the WPU solution, an electrostatic attraction was induced between the positively charged AEMA-GNs and the negatively charged sulfonate functional groups of WPU, as shown in Figure 1b. The strong interaction between the AEMA-GNs and WPU resulted in a homogeneous and stable dispersion of AEMA-GNs in the WPU matrix, facilitating the formation of conductive networks of GNs. In addition, this study investigated the effects of surface functional groups and the loading of GNs on the morphologies, electrical conductivities, and EMI SEs of the composites.

2. EXPERIMENTAL SECTION

2.1. Materials. Nano graphites (NGPs) synthesized via a chemical vapor deposition process were supplied by Angstron Materials LLC, Dayton, OH, USA. The thickness of the NGPs was less than 100 nm. Potassium permanganate ($KMnO_4$), sodium nitrate ($NaNO_3$), hydrogen peroxide (H_2O_2), potassium peroxodisulfate (KPS), sulfuric acid (H_2SO_4), and diethanolamine (DEA) were obtained from the Showa Chemical Co., Tokyo, Japan. Hexamethylene diisocyanate (HDI) was purchased from the Tokyo Chemical Industry Co., Ltd., Tokyo, Japan. 2-Aminoethyl methacrylate hydrochloride (AEMA monomer) was purchased from Sigma-Aldrich Co. LLC., St. Louis, MO, USA. Hydrazine (N_2H_4) was purchased from Alfa Aesar GmbH & Co. KG, Karlsruhe, Germany. YA-7720 (Mw 2000, 96 wt %) was obtained from the Coating Chemical Industry Co., Ltd., Taichung, Taiwan. *N*-(Ethylene sulfonate sodium salt) ethylene diamine (EES-200L, 45 wt %) was obtained from the Jiuh Yi Chemical Industry Co., Ltd., Taipei, Taiwan.

2.2. Preparation of Pristine-GNs (P-GNs). A modified Hummers method[32,33] was used to oxidize the NGPs to graphene oxide (GO). NGP (2 g), $NaNO_3$ (1.8 g), and 120 mL of H_2SO_4 were placed in a three-necked 500 mL flask and magnetically stirred at 0−3 °C in an ice bath until the NGPs and $NaNO_3$ completely dissolved. Subsequently, 10 g of $KMnO_4$ was gradually added to the mixture at room temperature, and the mixture was stirred to obtain a highly viscous fluid. The temperature of the mixture was then increased to 80 °C, and deionized water (DI water) was slowly added to the viscous mixture. Finally, H_2O_2 (15 wt %) was added to the mixture, which was then continuously stirred for 2 h. To obtain a pure GO solution, the liquid was purified by centrifuging 10 times at 10,000 rpm. The GO solution was dried under vacuum at 40 °C for 48 h to obtain a brown powder. After GO was dried, the sample was flushed with an inert gas (argon) for 10 min, and a quartz tube was quickly inserted into a furnace preheated to 970 °C and held in the furnace for 30 s,[34] and P-GN was obtained.

2.3. Preparation of AEMA-GNs Using Free Radical Polymerization. Figure 1a presents an overview of the covalent functionalization procedure. P-GN (1 g) was first suspended in 200 mL of DI water by subjecting the mixture to magnetic stirring for 1 h and sonication for 2 h. A mixture of AEMA monomer (1 g) and KPS (10 mg) in a 1:100 weight ratio was then dissolved in 50 mL of DI water and added to the GN suspension. Free radical polymerization was conducted with a nitrogen purge and vigorous stirring at 80 °C for 8 h. The product (1:1 AEMA-GN) was isolated by centrifugation and thoroughly washed 10 times with DI water to remove excess reactants. Finally, the 3:1 AEMA-GN product was prepared using 3 g of AEMA monomer via the aforementioned method. In addition, poly(AEMA) was synthesized using the aforementioned method.

2.4. Fabrication of GN/WPU Composites. First, YA-7720 (100 g) and HDI (10.08 g) were added to a four-necked reactor equipped with a mechanical stirrer, which was placed in an oil bath at 90 °C. When the prepolymer reaction was completed, the temperature was decreased to 40 °C, and acetone was added to the mixture to dissolve the prepolymer. The reactants [N_2H_4 (0.168 g), EES-200L (1.267 g), and DEA (0.210 g)] were slowly added to the reactor and reacted for 1 h. DI water (200 mL) was then slowly added to the reactor, and the mixture was stirred at 30 °C. Finally, the acetone was removed using a rotary evaporator to obtain a WPU aqueous solution with a concentration of 100 g/330 mL.

The composites were prepared via solution mixing. A P-GN (or AEMA-GN) solution was added to WPU solutions with various GN loadings. The GNs (or AEMA-GNs) were then dispersed in the WPU using a high-shear mixer at room temperature for 1 h. The composites were cast in Teflon molds, and the remaining moisture in the composites was removed by placing them in a vacuum oven at 80 °C. Finally, the P-GN/WPU (or AEMA-GN/WPU) composites were obtained.

2.5. Characterization. A high resolution X-ray photoelectron spectrometer (XPS) (ESCA pHI 1600, Physical Electronics, USA) was used to detect the detail of surface elements. Raman spectra were recorded from 1000 to 2000 cm^{-1} using a Stellar-PRO confocal Raman microscopy system (MODU-LASER, LLC), and the laser wavelength was 488 nm. Transmission electron microscopy (TEM) images were recorded using a JEM-2100 electron microscope operating at 200 kV, and the samples for the TEM measurements were prepared by drop casting a single drop onto lacey coated copper grids followed by solvent evaporation in air at room temperature. The thermal degradations of P-GN, 1:1 AEMA-GN, and 3:1 AEMA-GN were investigated using a thermogravimetric analyzer (TGA) (Hi-Res TGA 2950, TA Instruments, USA) from room temperature to 800 °C with a heating rate of 10 °C/min under a N_2 atmosphere (100 mL/min). A Malvern Zetasizer NanoZS system was used to measure the zeta potentials of P-GN, 1:1 AEMA-GN, and 3:1 AEMA-GN under acidic and neutral conditions with irradiation from a 632.8 nm He−Ne laser. The morphology of the polymer composites was imaged using a Hitachi field emitted-scanning electron microscope (FE-SEM) operating with an accelerating voltage of 15 kV. Samples were extracted from the flanges and fractured in liquid nitrogen, allowing analysis of the fractured surfaces, and were coated with 5 nm thick layer of gold (Cressington 208HR sputter coater) to limit charging effects during the investigation. The volume conductivities of the composites were measured using the four-point probe method (FPP-

DOI: 10.1021/am508069v
ACS Appl. Mater. Interfaces 2015, 7, 2817−2826

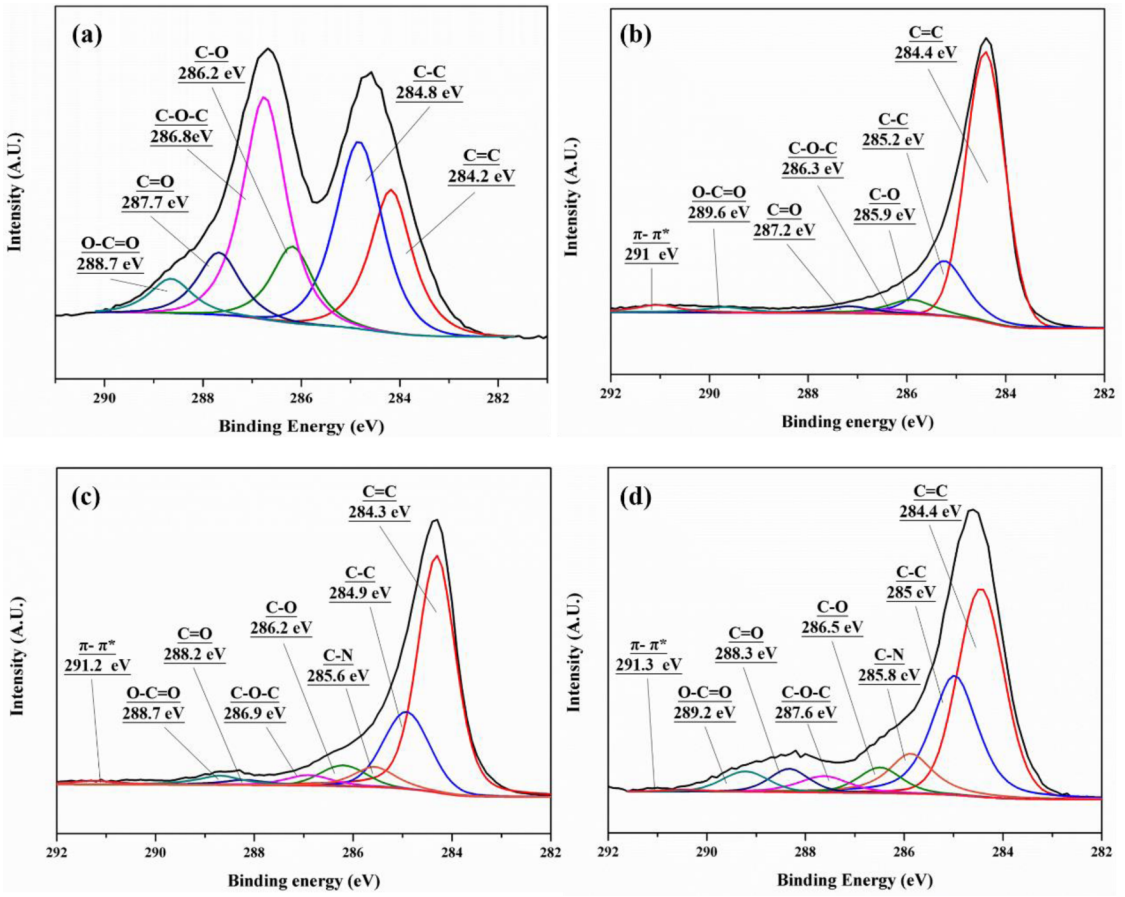

Figure 2. C 1s peaks in the XPS spectra of (a) GO, (b) P-GN, (c) 1:1 AEMA-GN, and (d) 3:1 AEMA-GN.

Table 1. Information Regarding the Distribution of Functional Groups Obtained from the XPS Spectra

	relative atomic percentage [%] (fitting of the C 1s peaks)							
sample	C═C	C−C	C−N	C−O	C−O−C	C═O	O−C═O	$\pi-\pi^*$
GO	19.3	27		10.1	30.5	8.3	4.5	
P-GN	66.5	18.3		5.7	1.2	3	2.4	2.9
1:1 AEMA-GN	58.5	20.9	4	6	3.5	2	3.6	1.5
3:1 AEMA-GN	40.1	26.9	9.6	5.2	4.1	9.6	4.1	0.4

5000, Miller Design Co. Woodside, Canada.). The average value was obtained from five measurements for each sample. For the low conductivity polymer composite (less than 10^{-6} S/m), the volume conductivity was measured using an SME-8311 MΩmeter (Dkk-Toa Co., Tokyo, Japan). A charge time of 20 s was applied, and the current stress during the measurements was 100 V. The average value was obtained from five measurements for each sample. EMI shielding measurements were conducted at room temperature over the frequency range of 8.2−12.4 GHz using an 8501C Vector Network Analyzer. The samples were cut into a coaxial circle with an inner diameter of 3.00 mm and outer diameter of 7.00 mm. To determine the shielding components for the composites, the scattering parameters, S_{11} and S_{21} were obtained. In general, the EMI SE of a composite is defined as the logarithmic ratio of the incident power, P_i, to the transmitted power, P_t, of the electromagnetic wave.[35]

$$SE_{total} = 10 \log(P_i/P_t) = -10 \log(1/|S_{21}|^2) \quad (1)$$

The unit for the EMI SE is decibels (dB). The higher the SE value in dB, the lower the energy passing through the material. The power coefficients of reflectivity (R), transmissivity (T), and absorptivity (A) can be calculated from the measured scattering parameters, and their relationship is described as $R + A + T = 1$.

$$T = |S_{21}|^2 \quad (2)$$

$$R = |S_{11}|^2 \quad (3)$$

SE_{total} is the sum of the SE that is due to absorption (SE_A), reflection (SE_R), and multiple reflection (SE_M).

$$SE_{total} = SE_A + SE_R + SE_M \quad (4)$$

When $SE_{total} > 10$ dB, SE_M can be neglected,[36] and it is generally assumed that

$$SE_{total} \sim SE_A + SE_R \quad (5)$$

Considering the effective absorbance, A_{eff}, with respect to the power of the incident electromagnetic wave inside the shielding material, the SE due to reflectance and effective absorption can be expressed as

$$A_{eff} = (1 - R - T)/(1 - R) \quad (6)$$

$$SE_R = -10 \log(1 - R) \quad (7)$$

$$SE_A = -10 \log(1 - A_{eff}) = -10 \log[T/(1 - R)] \quad (8)$$

DOI: 10.1021/am508069v
ACS Appl. Mater. Interfaces 2015, 7, 2817−2826

3. RESULTS AND DISCUSSION

3.1. Characterization of GO, P-GN, 1:1 AEMA-GN, and 3:1 AEMA-GN. XPS spectra were used to analyze the variation in the surface chemical composition of GO, P-GN, 1:1 AEMA-GN, and 3:1 AEMAGN. Figure 2 shows the C 1s core level spectra of these materials, and detailed information regarding the C 1s peaks is presented in Table 1. As shown in Figure 2a, the C 1s signal of GO clearly indicated a high degree of oxidation because of the low percentage of carbon/carbon bonds (aromatic C═C and aliphatic C−C) and the formation of oxygen-containing functional groups, including a hydroxyl carbon group, C−O; an epoxy group, C−O−C; a carbonyl group, C═O; and a carboxylate group, O−C═O. This result indicates that GO was successfully oxidized using the modified Hummers method. After thermal reduction, the number of oxygen-containing functional groups decreased significantly, and an increase in the carbon/carbon percentage was observed. Both the increased C═C percentage in P-GN (to 66.5%) and the appearance of the $\pi-\pi^*$ signal at 291 eV indicated that delocalized π conjugation was restored after thermal reduction, which was a critical factor in reducing the sheet resistance.[37,38] The C 1s XPS spectra of 1:1 AEMA-GNs and 3:1 AEMA-GNs, which are shown in Figures 2c and d, respectively, indicate that the percentage of the C═C peak decreased because the GNs were modified with AEMA through free radical polymerization; the C═C bonds of the GNs reacted with the radical functional groups induced by the initiator and transformed into C−C bonding. An additional peak at approximately 285.6 eV originating from the C−N functional group was observed and can be attributed to the backbone conformation of the AEMA segments. Increasing the amounts of AEMA monomers and initiators resulted in a decrease in the percentage of C═C bonds and an increase in the percentages of C−C and C−N bonds. Furthermore, the C 1s XPS spectra of 1:1 AEMA-GN and 3:1 AEMA-GN still possessed the $\pi-\pi^*$ signal at approximately 291.2 eV, indicating that the graphitic structures of 1:1 AEMA-GN and 3:1 AEMA-GN were not considerably damaged during free radical polymerization, which is beneficial for sustaining the electrical conductivity of AEMA-GNs. These results indicated that AEMA segments can be successfully grafted onto the GN surface through free radical polymerization of the AEMA monomer and the initiator to obtain the desired AEMA-GN structure.

Raman spectroscopy is a powerful tool for indicating the structural changes in GN materials through the D band (at approximately 1355 cm^{-1}, breathing mode of A1g) and G band (at approximately 1590 cm^{-1}, the in-plane bond-stretching motion of pairs of C sp^2 atoms, E2g mode),[39] as shown in Figure 3. The intensity ratio (I_D/I_G) between the sp^2 (G band) and sp^3 (D band) hybridization in the graphitic lattice can be used to determine the degree of modification, as shown in Table S1 (Supporting Information). The I_D/I_G ratio of P-GN was calculated to be 0.79, which corresponds to a two-dimensional sp^2 hybridized carbon sheet and the coexistence of sp^3 carbon in the basal edges or inside of defects in the planes.[21] After the GNs were modified with AEMA, the I_D/I_G ratio increased to 0.86 and 1.03 with respect to the different amounts of grafted AEMA. The initiator reacted with the AEMA monomer to produce radicals that react with the sp^2 graphitic carbon atoms in the GNs. Therefore, the attachment of AEMA segments was directly indicated by the higher I_D/I_G ratio compared with that of the P-GN. In addition, the I_D/I_G ratio of 3:1 AEMA-GN was higher than that of 1:1 AEMA-GN,

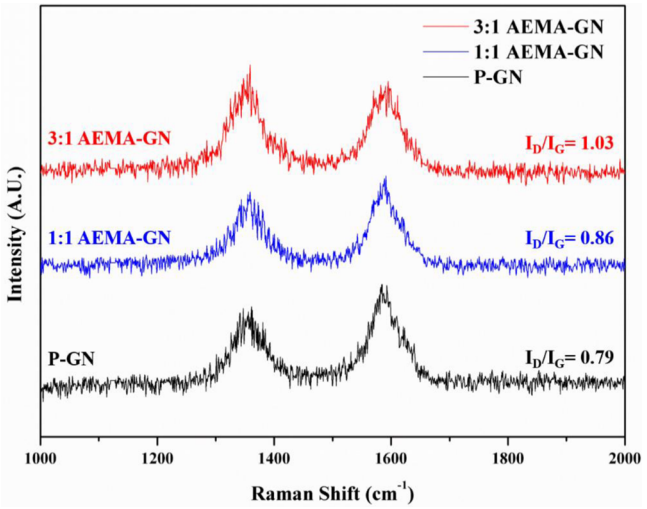

Figure 3. Raman spectra of P-GN, 1:1 AEMA-GN, and 3:1 AEMA-GN.

indicating that more AEMA segments grafted onto the GNs. Nevertheless, the G bands of the AEMA-GNs did not considerably broaden compared to those of P-GN. This comparison revealed that the graphitic structure of the AEMA-GNs was not severely disturbed as a result of the modification.

TEM was used to observe the surface morphologies of P-GN, 1:1 AEMA-GN, and 3:1 AEMA-GN. Figure 4a presents the

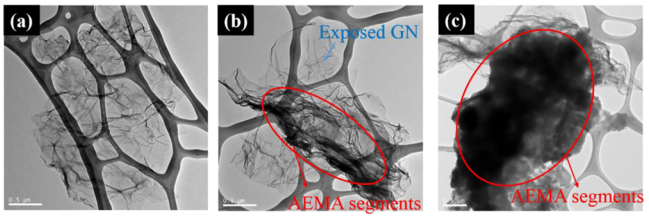

Figure 4. TEM images of (a) P-GN, (b) 1:1 AEMA-GN, and (c) 3:1 AEMA-GN.

TEM morphology for P-GN. Because of the effective thermal expansion of GO, the P-GN exhibited an exceptionally thin and uneven texture, indicating that the P-GN was highly reduced. The morphologies of 1:1 AEMA-GN and 3:1 AEMA-GN (Figure 4b and c) clearly differed from that of P-GN, and the AEMA-GNs were both covered with dark and gray clouds. These variations can be attributed to the AEMA segments being aligned on the surfaces of the GNs. In contrast, the 3:1 AEMA-GN was almost completely covered with AEMA segments without exposed GN, indicating a high degree of modification of 3:1 AEMA-GN. Furthermore, the TEM results indicated that the AEMA-GNs were successfully modified using AEMA through free radical polymerization without destroying the structure of the GNs.

To further investigate the modification of the GNs, TGA measurements were used to determine the content of grafted AEMA on the GNs. The TGA curves of poly(AEMA), P-GN, 1:1 AEMA-GN, and 3:1 AEMA-GN are shown in Figure 5, and these measurements were conducted under a nitrogen purge. The P-GN exhibited high thermal stability and no obvious weight loss in the tested temperature range, indicating that the residual oxygen-containing functional groups were removed.

DOI: 10.1021/am508069v
ACS Appl. Mater. Interfaces 2015, 7, 2817−2826

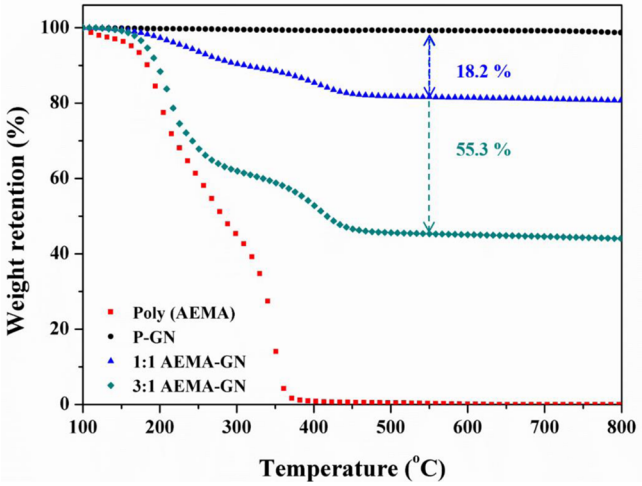

Figure 5. TGA curves of poly(AEMA), P-GNS, 1:1 AEMA-GN, and 3:1 AEMA-GN.

However, poly(AEMA) completely decomposes above 550 °C. For 1:1 AEMA-GN and 3:1 AEMA-GN, the AEMA segments on AEMA-GNs were clearly degraded between 200 and 450 °C. The slower thermal degradation rate of these materials compared with poly(AEMA) can be attributed to the action of the GNs as free radical acceptors during the thermal decomposition of the AEMA segments.[40,41] Compared with the GN and poly(AEMA), the grafting ratios of 1:1 AEMA-GN and 3:1 AEMA-GN were calculated to be 18.2 and 55.3 wt %, respectively, suggesting that the GNs were successfully modified with AEMA through free radical polymerization. The observation that the GNs were modified with AEMA was consistent with the results of the XPS and TEM investigations.

To improve the compatibility between the GNs and WPU, AEMA was used to modify the GNs through free radical polymerization. The grafted AEMA polymer chains in AEMA-GNs consist of many $-NH_2$ functional groups, which become $-NH_3^+$ functional groups in an acidic environment. The zeta potential is a useful parameter for analyzing the electrostatic interactions of GN aqueous solution.[42,43] As shown in Figure 6, the zeta potentials of P-GN were determined to be −2.8 mV and −1.3 mV under neutral (pH 7) and acidic (pH 3) conditions, respectively, indicating the presence of residual

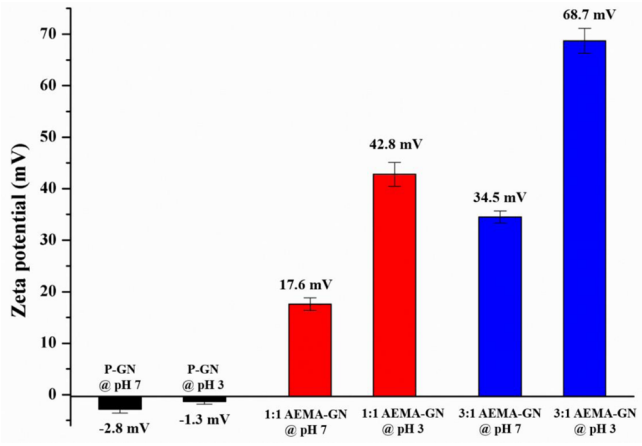

Figure 6. Zeta potential measurements of AEMA, P-GNS, 1:1 AEMA-GN, and 3:1 AEMA-GN.

oxygen-containing functional groups on the P-GNs. The low zeta potential of P-GN made stably dispersing the P-GNs in aqueous solution difficult.[43] After modification with AEMA, the zeta potentials of both AEMA-GNs became positive. Under neutral conditions, the zeta potentials of 1:1 AEMA-GN and 3:1 AEMA-GN were 17.6 and 34.5 mV, respectively. However, the zeta potentials of the AEMA-GNs became more positive (42.8 mV for 1:1 AEMA-GN and 68.7 mV for 3:1 AEMA-GN) under acidic conditions (pH 3) because a large amount of $-NH_2$ functional groups of the grafted AEMA segments converted into $-NH_3^+$ functional groups. The highly positively charged AEMA-GNs not only effectively inhibit the restacking and aggregation of GNs but also exhibit high compatibility with the negatively charged WPU matrix.

3.2. Morphologies of P-GN/WPU and AEMA-GN/WPU Composites. The dispersion state of the nanofillers in the polymer matrix strongly influences the performance of composites, particularly the electrical conductivity.[18] Therefore, the dispersion and compatibility of the fillers in the polymer matrix were investigated using SEM by observing the fractured surface morphologies of the composites. As shown in Figure 7a,

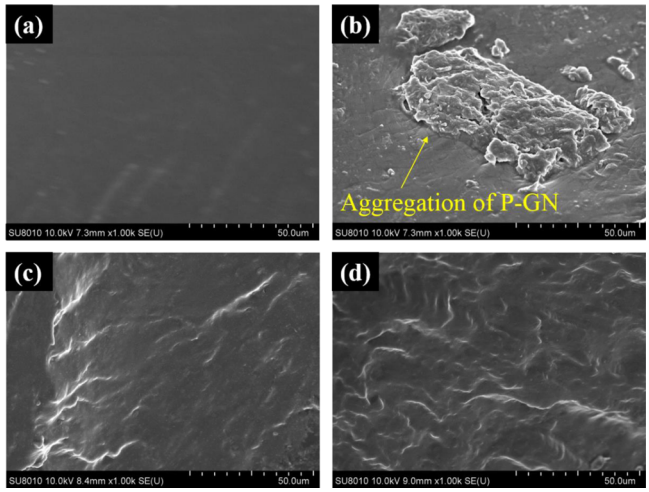

Figure 7. SEM images of the fractured surfaces of (a) WPU; (b) P-GN/WPU containing 1 vol % P-GN (the red arrows indicate that the P-GN was pulled out from the WPU matrix and aggregated because of poor compatibility); (c) 1:1 AEMA-GN/WPU containing 1 vol % 1:1 AEMA-GN; and (d) 3:1 AEMA-GN/WPU containing 1 vol % 3:1 AEMA-GN.

the neat WPU exhibited a fairly fractured surface. Figure 7b presents the fractured surfaces of 1 vol % P-GN/WPU composites. P-GNs were pulled out from the WPU matrix, indicating weak adhesion and poor compatibility between the P-GNs and WPU matrix. In addition, the poor compatibility caused the P-GNs to strongly aggregate, resulting in limited reinforcement of WPU. Compared with the P-GN/WPU composites, the AEMA-GN/WPU composites exhibited a rougher surface, and the AEMA-GNs were both homogeneously dispersed and embedded in the WPU matrix and did not aggregate or get pulled out directly under tension. In contrast, the fracture surface of 3:1 AEMA-GN/WPU was rougher than that of 1:1 AEMA-GN/WPU, indicating that the 3:1 AEMA-GNs exhibited stronger interfacial interactions with the WPU matrix than did the 1:1 AEMA-GNs. Because of the high degree of modification and coverage of the AEMA segments, the 3:1 AEMA-GN possessed large amounts of

DOI: 10.1021/am508069v
ACS Appl. Mater. Interfaces 2015, 7, 2817−2826

$-NH_3^+$ functional groups, which exhibited stronger interfacial adhesion and higher compatibility with the WPU matrix grafted with negatively charged sulfonate functional groups. Consequently, the AEMA-GNs were both homogeneously dispersed and interconnected with each other, facilitating the formation of GN networks. The formation of GN networks is anticipated to play an important role in enhancing the electrical conductivities of polymer composites.

3.3. Electrical Conductivities of GN/WPU and AEMA-GN/WPU Composites. The electrical conductivity of composites plays a vital role in improving the EMI shielding properties.[5,15] Figure 8 presents the electrical conductivities of the P-GN/WPU, 1:1 AEMA-GN/WPU, and 3:1 AEMA-GN/WPU composites with various GN loadings; all of the composites became electrically conductive from insulating at low GN loadings. The electrical conductivities of the composites exhibited a considerable increase because of the formation of electrically conductive GN networks. As shown in Figure 8, the electrical conductivities of the composites increased from 6.56×10^{-15} S/m to 1.78 S/m with 5 vol % GN, to 43.64 S/m with 5 vol % 1:1 AEMA-GN, and to 13.2 S/m with 5 vol % 3:1 AEMA-GN. As shown in Figure 8, the AEMA-GN/WPU composites exhibited a significant improvement in electrical conductivity and a low percolation threshold compared with those of P-GNs. This result can be attributed to the improved dispersion of AEMA-GNs in the WPU matrix, which facilitates the formation of an interconnected GN conductive network. In comparison, the 3:1 AEMA-GN/WPU composite exhibited a lower percolation threshold than did the 1:1 AEMA-GN/WPU composite because the compatibility between the 3:1 AEMA-GNs and the WPU matrix was better; this result is consistent with the results of the morphology observations conducted using SEM. However, at a GN loading of 5 vol %, the electrical conductivity of 1:1 AEMA-GN/WPU (43.64 S/m) was higher than that of 3:1 AEMA-GN/WPU (13.2 S/m). Because the graphitic sp^2 structure (C=C bonding) of 3:1 AEMA-GN/WPU was less complete than that of 1:1 AEMA-GN/WPU, the disrupted graphitic structure reduced the intrinsic electrical conductivity. In addition, the high coverage of insulated AEMA segments on 3:1 AEMA-GN hindered electron transport among the GNs, thereby reducing the electrical conductivity.

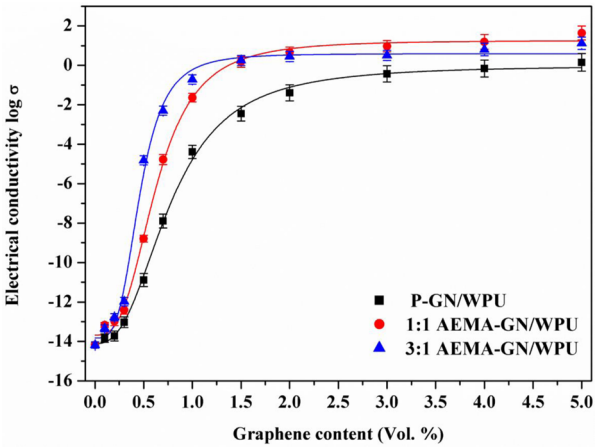

Figure 8. Electrical conductivities of P-GN/WPU, 1:1 AEMA-GN/WPU, and 3:1 AEMA-GN/WPU composites with varying GN contents.

3.4. EMI Shielding Properties of P-GN/WPU and AEMA-GN/WPU Composites. The EMI SE and mechanism of conductive composites are major factors for indicating the potential applications for the lightweight and conductive GN/WPU composites. As shown in Figure 9, the EMI SEs of P-GN/WPU, 1:1 AEMA-GN/WPU, and 3:1 AEMA-GN/WPU composites with various GN loadings over the frequency range of 8.2−12.4 GHz were measured and compared. In general, an EMI SE value of 20 dB is considered adequate for commercial applications of EMI shielding materials.[12] Because of the highly insulating property of WPU, it exhibits no EMI shielding ability. The EMI SEs of the composites were markedly enhanced by increasing GN loadings; this observation was consistent with the results regarding the electrical conductivities of the composites. As shown in Figure 9, the EMI SE values of the P-GN/WPU, 1:1 AEMA-GN/WPU, and 3:1 AEMA-GN/WPU composites at a GN loading of 2 vol % were 7, 19, and 20 dB, respectively. When the GN loading was increased to 5 vol %, the SE values of the P-GN/WPU, 1:1 AEMA-GN/WPU, and 3:1 AEMA-GN/WPU composites were 18, 33, and 38 dB, respectively. The EMI SE values of the composites are considerably higher than that of commercially available EMI shielding materials.

In contrast, the EMI SEs of both AEMA-GN/WPU composites were higher than that of the P-GN/WPU composite with the same GN loading. The presence of AEMA segments on the AEMA-GNs ensures that the compatibility with the WPU matrix is high because the electrostatic attraction causes the incorporated GNs to become homogeneously dispersed in the WPU matrix, thereby improving the EMI shielding performance of the composites.[44,45]

The increase in the EMI SE of 3:1 AEMA-GN/WPU was higher than that of 1:1 AEMA-GN/WPU when the GN loading was less than 2 vol % because the 3:1 AEMA-GNs formed electrically conductive networks more effectively than did the 1:1 AEMA-GNs. This result is similar to those regarding the electrical conductivities of the composites. However, when the GN loading was increased to more than 2 vol %, the increase in the EMI SE of 3:1 AEMA-GN/WPU was lower than that in the SE of 1:1 AEMA-GN/WPU. The high concentration of AEMA segments grafted on the 3:1 AEMA-GN/WPU reduced the intrinsic electrical conductivity of the GN structure, thus limiting the improvement in the EMI shielding performance.[46]

Figure 10 presents a comparison of the EMI SE_{total}, absorption (SE_A), and reflection (SE_R) between AEMA-GNS/WPU composites with different GN loadings at 9.6 GHz. The absorption depends on the electric or magnetic dipoles interacting with the incident electromagnetic wave. As for reflection, the shielding material surface, which has mobile charge carriers, interacts with electromagnetic field in the radiation.[11] As shown in Figure 10, both the SE_{total} and SE_A of the two composites increased as the GN loading increased, but SE_R increased only slightly. In addition, the improvements in the SE_A of the composites were consistent with the growth trend of the SE_{total}, and the contribution of absorption to SE_{total} was greater than that of the reflection. Absorption was observed to have a dominant contribution of EMI shielding performance, which has been predicted theoretically and exhibited experimentally with increased frequency, as shown in Figure S2 (Supporting Information). A similar shielding mechanism was also observed in a previous study.[11,15,16,46] The incident electromagnetic wave was dissipated by the conduction induced

DOI: 10.1021/am508069v
ACS Appl. Mater. Interfaces 2015, 7, 2817−2826

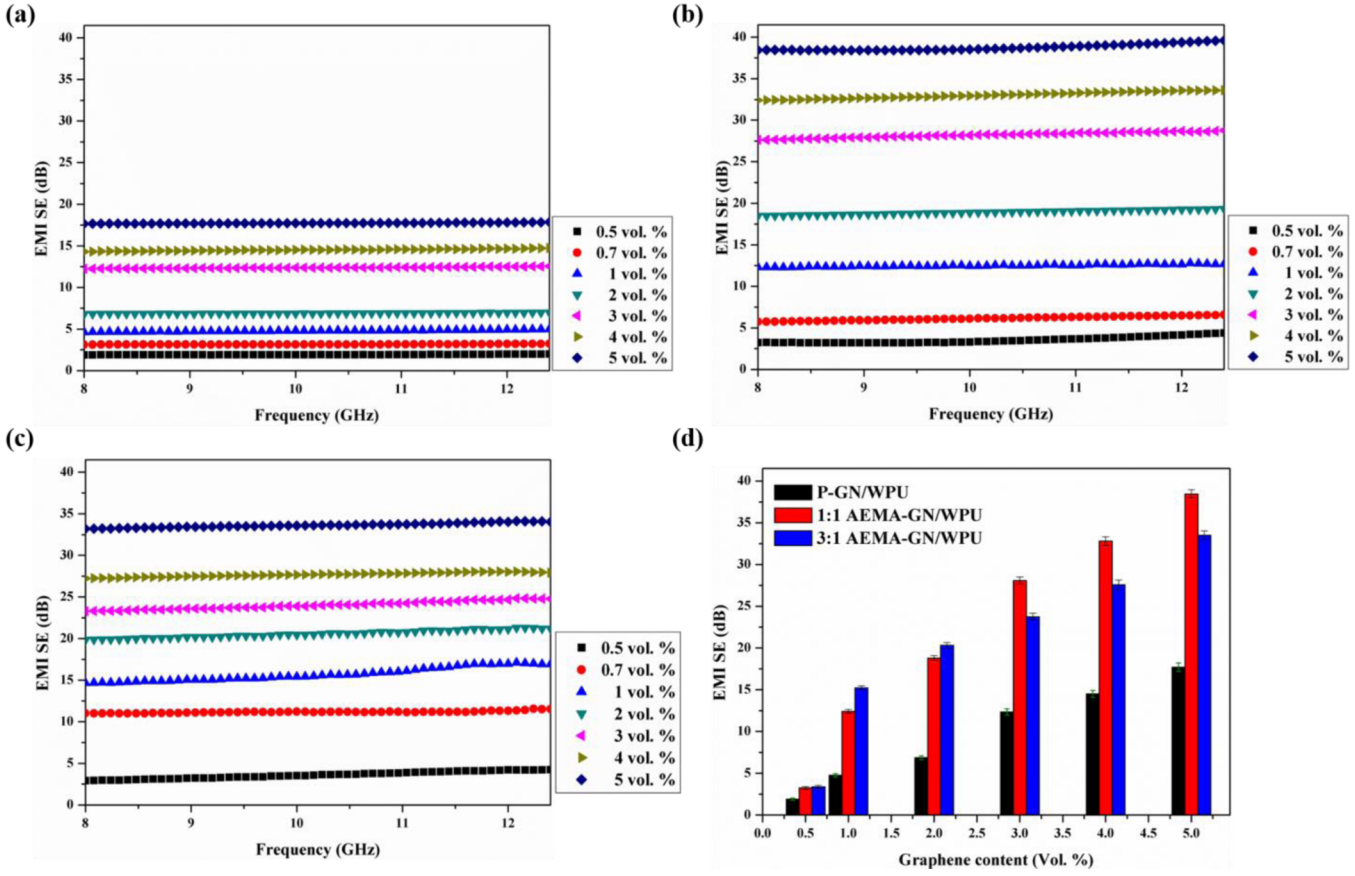

Figure 9. EMI SE of the (a) P-GN/WPU, (b) 1:1 AEMA-GN/WPU, and (c) 3:1 AEMA-GN/WPU composites with varying GN contents. (d) Comparison of the EMI SE of the P-GN/WPU, 1:1 AEMA-GN/WPU, and 3:1 AEMA-GN/WPU composites with various GN loadings at 9.6 GHz.

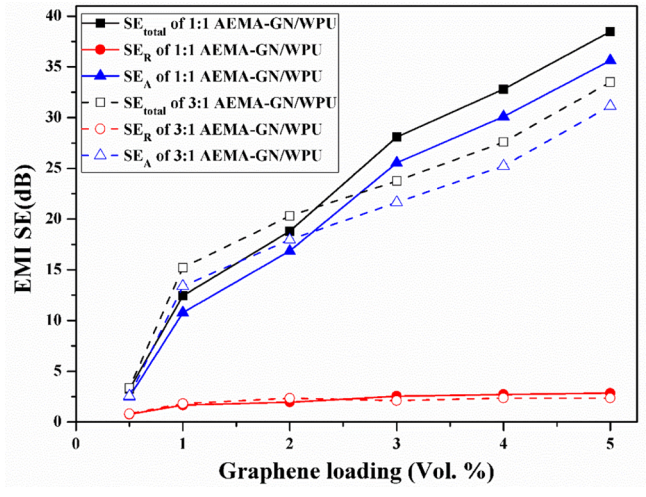

Figure 10. Comparison of the SE_{total}, SE_A, and SE_R of the 1:1 AEMA-GN/WPU and 3:1 AEMA-GN/WPU composites with different GN loadings at 9.6 GHz.

by the GN networks inside the composites. Because of the good compatibility between the AEMA-GNs and the WPU matrix, AEMA-GNs were homogeneously dispersed in the WPU matrix, which facilitated the formaiton of conductive networks. The formed conductive networks can effectively mobilize the charge carriers in the WPU matrix, causing the incident electromagnetic wave to dissipate and improving the SE_A of the shielding material. Increasing GN loading facilitates the formation of more complex conductive networks in the WPU matrix, thus promoting the dissipation of incident electromagnetic wave and increasing the absorption (SE_A) of the shielding material.

The SE_{total} was dominated by SE_A, which can be attributed to the electrical conductivity and dispersion state of the AEMA-GNs in the WPU matrix. The conductive networks in the 3:1 AEMA-GN/WPU composite can be formed using a lower GN content than that used for the formation of conductive networks in 1:1 AEMA-GN/WPU composite because 3:1 AEMA-GNs exhibit stronger interactions and higher compatibility with the WPU matrix. However, at higher GN loadings, the 1:1 AEMA-GN/WPU composite exhibited a higher SE_{total} and SE_A than did the 3:1 AEMA-GN/WPU composite; this observation is consistent with the results regarding the electrical conductivities of the composites. The large amount of AEMA segments on 3:1 AEMA-GN destroys the intrinsic sp^2 bonding, which disturbs the mobility of charge carriers, thereby reducing the dissipation of electromagnetic waves. In addition, the high concentration of AEMA segments on the GN surface hinders the contact among GNs, and the movement of charge carriers among GNs becomes difficult. Compared with 3:1 AEMA-GNs, the graphitic structure of 1:1 AEMA-GNs is more complete, causing the intrinsic conductivity to be higher; the charge carriers can easily move among GNs because the concentration of AEMA segments on 1:1 AEMA-GNs is lower. Furthermore, the lower AEMA coverage on GNs improved the polarity of 1:1 AEMA-GN, thereby enhancing the intrinsic shielding performance of the GNs.[46−48] Thus, 1:1 AEMA-GNs

DOI: 10.1021/am508069v
ACS Appl. Mater. Interfaces 2015, 7, 2817−2826

in WPU composites can be used to more effectively dissipate incident electromagnetic waves than 3:1AEMA-GNs.

4. CONCLUSIONS

This study demonstrated the effect of covalent modification of GN for improving the electrical conductivities and EMI shielding properties of GN/WPU composites. To improve the compatibility of the GNs with the WPU matrix, AEMA was grafted onto the surface of the GNs through free radical polymerization. The $-NH_3^+$ functional groups of the AEMA segments on the AEMA-GNs exhibited strong compatibility with WPU through electrostatic attractions. Because of the high compatibility of the AEMA-GNs with the WPU matrix, the AEMA-GNs exhibited homogeneous dispersion without aggregation and still maintain a high surface area in the WPU matrix. In addition, AEMA-GNs with various concentrations of AEMA segments were discussed. Because of the higher concentration of grafted AEMA segments on 3:1 AEMA-GNs, the 3:1 AEMA-GNs exhibited stronger interaction and higher compatibility with the WPU matrix, and a lower percolation threshold of electrical conductivity than did the 1:1 AEMA-GNs. However, the graphitic structure of 3:1 AEMA-GN was less complete than that of 1:1 AEMA-GN. The disturbed graphitic structure limited the intrinsic electrical conductivity of the GNs. Moreover, the high concentration of AEMA segments on the GNs limited the mobility of electrons. Although the 1:1 AEMA-GNs exhibited a higher percolation threshold in the WPU matrix than did the 3:1 AEMA-GNs, the 1:1 AEMA-GN/WPU composites with a GN loading of 5 vol % exhibited a high electrical conductivity (43.64 S/m) and a high EMI SE (38 dB) in the X-band frequency range. Consequently, the electrical conductivity and EMI shielding performance of these composites can be influenced by the compatibility between the GNs and the polymer matrix and by the integrity of the graphitic structure of the GNs. The surface modification of GNs provides new directions for the development of lightweight and high performance electrically conductive polymer composites for use as high-performance EMI shielding materials.

■ ASSOCIATED CONTENT

Supporting Information

Raman data of P-GN, 1:1 AEMA-GN, and 3:1 AEMA-GN and the in-plane crystallite sizes; aging effect test on electromagnetic shielding performance of composites; and absorption (SEA) and reflection (SER) of shielding for composites. This material is available free of charge via the Internet at http://pubs.acs.org.

■ AUTHOR INFORMATION

Corresponding Author

*Tel: 886-3-5713058. Fax: 886-3-5715408. E-mail: ccma@che.nthu.edu.tw.

Notes

The authors declare no competing financial interest.

■ ACKNOWLEDGMENTS

The authors thank National Science Council, Taiwan for financially supporting this research (NSC 102-2221-E-007-003-102 and NSC 103-2221-E-007-130-(103).

■ REFERENCES

(1) Watts, P. C. P.; Hsu, W. K.; Barnes, A.; Chambers, B. High permittivity from defective multiwalled carbon nanotubes in the X-band. *Adv. Mater.* **2003**, *15* (7−8), 600−603.

(2) Singh, A. P.; Garg, P.; Alam, F.; Singh, K.; Mathur, R. B.; Tandon, R. P.; Chandra, A.; Dhawan, S. K. Phenolic resin-based composite sheets filled with mixtures of reduced graphene oxide, gamma-Fe2O3 and carbon fibers for excellent electromagnetic interference shielding in the X-band. *Carbon* **2012**, *50* (10), 3868−3875.

(3) Huang, Y.; Li, N.; Ma, Y.; Du, F.; Li, F.; He, X.; Lin, X.; Gao, H.; Chen, Y. The influence of single-walled carbon nanotube structure on the electromagnetic interference shielding efficiency of its epoxy composites. *Carbon* **2007**, *45* (8), 1614−1621.

(4) Eswaraiah, V.; Sankaranarayanan, V.; Ramaprabhu, S. Functionalized graphene−PVDF foam composites for EMI shielding. *Macromol. Mater. Eng.* **2011**, *296* (10), 894−898.

(5) Chung, D. Electromagnetic interference shielding effectiveness of carbon materials. *Carbon* **2001**, *39* (2), 279−285.

(6) Liang, J.; Wang, Y.; Huang, Y.; Ma, Y.; Liu, Z.; Cai, J.; Zhang, C.; Gao, H.; Chen, Y. Electromagnetic interference shielding of graphene/epoxy composites. *Carbon* **2009**, *47* (3), 922−925.

(7) Liu, X.; Yin, X.; Kong, L.; Li, Q.; Liu, Y.; Duan, W.; Zhang, L.; Cheng, L. Fabrication and electromagnetic interference shielding effectiveness of carbon nanotube reinforced carbon fiber/pyrolytic carbon composites. *Carbon* **2014**, *68*, 501−510.

(8) Joo, J.; Lee, C. High frequency electromagnetic interference shielding response of mixtures and multilayer films based on conducting polymers. *J. Appl. Phys.* **2000**, *88* (1), 513−518.

(9) Zhang, H.-B.; Zheng, W.-G.; Yan, Q.; Yang, Y.; Wang, J.-W.; Lu, Z.-H.; Ji, G.-Y.; Yu, Z.-Z. Electrically conductive polyethylene terephthalate/graphene nanocomposites prepared by melt compounding. *Polymer* **2010**, *51* (5), 1191−1196.

(10) Wen, B.; Cao, M.; Lu, M.; Cao, W.; Shi, H.; Liu, J.; Wang, X.; Jin, H.; Fang, X.; Wang, W. Reduced graphene oxides: light-weight and high-efficiency electromagnetic interference shielding at elevated temperatures. *Adv. Mater.* **2014**, *26*, 3484−3489.

(11) Gupta, T. K.; Singh, B. P.; Mathur, R. B.; Dhakate, S. R. Multi-walled carbon nanotube−graphene−polyaniline multiphase nanocomposite with superior electromagnetic shielding effectiveness. *Nanoscale* **2014**, *6* (2), 842−851.

(12) Al-Saleh, M. H.; Saadeh, W. H.; Sundararaj, U. EMI shielding effectiveness of carbon based nanostructured polymeric materials: a comparative study. *Carbon* **2013**, *60*, 146−156.

(13) Neto, A. C.; Guinea, F.; Peres, N.; Novoselov, K. S.; Geim, A. K. The electronic properties of graphene. *Rev. Mod. Phys.* **2009**, *81* (1), 109.

(14) Rao, C. N. R.; Sood, A. K.; Subrahmanyam, K. S.; Govindaraj, A. Graphene: The new two-dimensional nanomaterial. *Angew. Chem., Int. Ed.* **2009**, *48* (42), 7752−7777.

(15) Chen, Z.; Xu, C.; Ma, C.; Ren, W.; Cheng, H. M. Lightweight and flexible graphene foam composites for high-performance electromagnetic interference shielding. *Adv. Mater.* **2013**, *25*, 1296−1300.

(16) Wen, B.; Wang, X.; Cao, W.; Shi, H.; Lu, M.; Wang, G.; Jin, H.; Wang, W.; Yuan, J.; Cao, M. Reduced graphene oxides: the thinnest and most lightweight materials with highly efficient microwave attenuation performances of the carbon world. *Nanoscale* **2014**, *6*, 5754−5761.

(17) Ma, J.; Meng, Q.; Michelmore, A.; Kawashima, N.; Izzuddin, Z.; Bengtsson, C.; Kuan, H.-C. Covalently bonded interfaces for polymer/graphene composites. *J. Mater. Chem. A* **2013**, *1* (13), 4255−4264.

(18) Kuilla, T.; Bhadra, S.; Yao, D.; Kim, N. H.; Bose, S.; Lee, J. H. Recent advances in graphene based polymer composites. *Prog. Polym. Sci.* **2010**, *35* (11), 1350−1375.

(19) Ma, J.; Meng, Q.; Zaman, I.; Zhu, S.; Michelmore, A.; Kawashima, N.; Wang, C. H.; Kuan, H.-C. Development of polymer composites using modified, high-structural integrity graphene platelets. *Compos. Sci. Technol.* **2014**, *91*, 82−90.

(20) Hsiao, M.-C.; Liao, S.-H.; Yen, M.-Y.; Liu, P.-I.; Pu, N.-W.; Wang, C.-A.; Ma, C.-C. M. Preparation of covalently functionalized

DOI: 10.1021/am508069v
ACS Appl. Mater. Interfaces 2015, 7, 2817−2826

graphene using residual oxygen-containing functional groups. *ACS Appl. Mater. Interfaces* **2010**, *2* (11), 3092−3099.
(21) Georgakilas, V.; Otyepka, M.; Bourlinos, A. B.; Chandra, V.; Kim, N.; Kemp, K. C.; Hobza, P.; Zboril, R.; Kim, K. S. Functionalization of graphene: covalent and non-covalent approaches, derivatives and applications. *Chem. Rev.* **2012**, *112* (11), 6156−6214.
(22) Kuila, T.; Bose, S.; Mishra, A. K.; Khanra, P.; Kim, N. H.; Lee, J. H. Chemical functionalization of graphene and its applications. *Prog. Mater. Sci.* **2012**, *57* (7), 1061−1105.
(23) Vasileiou, A. A.; Kontopoulou, M.; Docoslis, A. A non-covalent compatibilization approach to improve the filler dispersion and properties of polyethylene/graphene composites. *ACS Appl. Mater. Interfaces* **2014**, *6*, 1916−1925.
(24) Teng, C.-C.; Ma, C.-C. M.; Lu, C.-H.; Yang, S.-Y.; Lee, S.-H.; Hsiao, M.-C.; Yen, M.-Y.; Chiou, K.-C.; Lee, T.-M. Thermal conductivity and structure of non-covalent functionalized graphene/epoxy composites. *Carbon* **2011**, *49* (15), 5107−5116.
(25) Hsiao, S.-T.; Ma, C.-C. M.; Tien, H.-W.; Liao, W.-H.; Wang, Y.-S.; Li, S.-M.; Huang, Y.-C. Using a non-covalent modification to prepare a high electromagnetic interference shielding performance graphene nanosheet/water-borne polyurethane composite. *Carbon* **2013**, *60* (0), 57−66.
(26) Lu, Y.; Tighzert, L.; Dole, P.; Erre, D. Preparation and properties of starch thermoplastics modified with waterborne polyurethane from renewable resources. *Polymer* **2005**, *46* (23), 9863−9870.
(27) Wicks, Z. W., Jr.; Wicks, D. A.; Rosthauser, J. W. Two package waterborne urethane systems. *Prog. Org. Coat.* **2002**, *44* (2), 161−183.
(28) Bao, L.-H.; Lan, Y.-J.; Zhang, S.-F. Synthesis and properties of waterborne polyurethane dispersions with ions in the soft segments. *J. Polym. Res.* **2006**, *13* (6), 507−514.
(29) Perez-Liminana, M.; Aran-Ais, F.; Torró-Palau, A. M.; César Orgilés-Barceló, A.; Miguel Martín-Martínez, J. Characterization of waterborne polyurethane adhesives containing different amounts of ionic groups. *Int. J. Adhes. Adhes.* **2005**, *25* (6), 507−517.
(30) Wen, T.-C.; Wang, Y.-J.; Cheng, T.-T.; Yang, C.-H. The effect of DMPA units on ionic conductivity of PEG−DMPA−IPDI waterborne polyurethane as single-ion electrolytes. *Polymer* **1999**, *40* (14), 3979−3988.
(31) Delpech, M. C.; Coutinho, F. Waterborne anionic polyurethanes and poly (urethane-urea) s: influence of the chain extender on mechanical and adhesive properties. *Polym. Test* **2000**, *19* (8), 939−952.
(32) Hummers, W. S., Jr.; Offeman, R. E. Preparation of graphitic oxide. *J. Am. Chem. Soc.* **1958**, *80* (6), 1339−1339.
(33) Hirata, M.; Gotou, T.; Horiuchi, S.; Fujiwara, M.; Ohba, M. Thin-film particles of graphite oxide 1:: High-yield synthesis and flexibility of the particles. *Carbon* **2004**, *42* (14), 2929−2937.
(34) McAllister, M. J.; Li, J.-L.; Adamson, D. H.; Schniepp, H. C.; Abdala, A. A.; Liu, J.; Herrera-Alonso, M.; Milius, D. L.; Car, R.; Prud'homme, R. K. Single sheet functionalized graphene by oxidation and thermal expansion of graphite. *Chem. Mater.* **2007**, *19* (18), 4396−4404.
(35) Wang, J.; Xiang, C.; Liu, Q.; Pan, Y.; Guo, J. Ordered mesoporous carbon/fused silica composites. *Adv. Funct. Mater.* **2008**, *18* (19), 2995−3002.
(36) Yuan, B. Q.; Yu, L. M.; Sheng, L. M.; An, K.; Zhao, X. L. Comparison of electromagnetic interference shielding properties between single-wall carbon nanotube and graphene sheet/polyaniline composites. *J. Phys. D Appl. Phys.* **2012**, *45*; DOI: 10.1088/0022-3727/45/23/235108.
(37) Ganguly, A.; Sharma, S.; Papakonstantinou, P.; Hamilton, J. Probing the thermal deoxygenation of graphene oxide using high-resolution in situ X-ray-based spectroscopies. *J. Phys. Chem. C* **2011**, *115* (34), 17009−17019.
(38) Paredes, J.; Villar-Rodil, S.; Solis-Fernandez, P.; Martinez-Alonso, A.; Tascon, J. Atomic force and scanning tunneling microscopy imaging of graphene nanosheets derived from graphite oxide. *Langmuir* **2009**, *25* (10), 5957−5968.
(39) Kudin, K. N.; Ozbas, B.; Schniepp, H. C.; Prud'Homme, R. K.; Aksay, I. A.; Car, R. Raman spectra of graphite oxide and functionalized graphene sheets. *Nano Lett.* **2008**, *8* (1), 36−41.
(40) Galano, A. Carbon nanotubes: promising agents against free radicals. *Nanoscale* **2010**, *2* (3), 373−380.
(41) Lin, Y.-C.; Lu, C.-C.; Yeh, C.-H.; Jin, C.; Suenaga, K.; Chiu, P.-W. Graphene annealing: how clean can it be? *Nano Lett.* **2011**, *12* (1), 414−419.
(42) Li, D.; Müller, M. B.; Gilje, S.; Kaner, R. B.; Wallace, G. G. Processable aqueous dispersions of graphene nanosheets. *Nature Nanotechnol.* **2008**, *3* (2), 101−105.
(43) Si, Y.; Samulski, E. T. Synthesis of water soluble graphene. *Nano Lett.* **2008**, *8* (6), 1679−1682.
(44) Fugetsu, B.; Sano, E.; Sunada, M.; Sambongi, Y.; Shibuya, T.; Wang, X.; Hiraki, T. Electrical conductivity and electromagnetic interference shielding efficiency of carbon nanotube/cellulose composite paper. *Carbon* **2008**, *46* (9), 1256−1258.
(45) Yang, Y.; Gupta, M. C.; Dudley, K. L.; Lawrence, R. W. Novel carbon nanotube-polystyrene foam composites for electromagnetic interference shielding. *Nano Lett.* **2005**, *5* (11), 2131−2134.
(46) Zhang, H.-B.; Zheng, W.-G.; Yan, Q.; Jiang, Z.-G.; Yu, Z.-Z. The effect of surface chemistry of graphene on rheological and electrical properties of polymethylmethacrylate composites. *Carbon* **2012**, *50* (14), 5117−5125.
(47) Vázquez, E.; Prato, M. Carbon nanotubes and microwaves: interactions, responses, and applications. *ACS Nano* **2009**, *3* (12), 3819−3824.
(48) Imholt, T.; Dyke, C.; Hasslacher, B.; Perez, J.; Price, D.; Roberts, J.; Scott, J.; Wadhawan, A.; Ye, Z.; Tour, J. Nanotubes in microwave fields: light emission, intense heat, outgassing, and reconstruction. *Chem. Mater.* **2003**, *15* (21), 3969−3970.

DOI: 10.1021/am508069v
ACS Appl. Mater. Interfaces 2015, 7, 2817−2826